High and low density patches in simulated liquid water

N. Ansari, R. Dandekar, S. Caravati, G.C. Sosso, and A. Hassanali

---

Articles you may be interested in

Perspective: Crossing the Widom line in no man's land: Experiments, simulations, and the location of the liquid-liquid critical point in supercooled water
The Journal of Chemical Physics **149**, 140901 (2018); 10.1063/1.5046687

Common microscopic structural origin for water's thermodynamic and dynamic anomalies
The Journal of Chemical Physics **149**, 224502 (2018); 10.1063/1.5055908

On the geometric dependence of the molecular dipole polarizability in water: A benchmark study of higher-order electron correlation, basis set incompleteness error, core electron effects, and zero-point vibrational contributions
The Journal of Chemical Physics **149**, 204303 (2018); 10.1063/1.5051458

Comment on "The putative liquid-liquid transition is a liquid-solid transition in atomistic models of water" [I and II: J. Chem. Phys. 135, 134503 (2011); J. Chem. Phys. 138, 214504 (2013)]
The Journal of Chemical Physics **148**, 137101 (2018); 10.1063/1.5029463

Perspective: Computational chemistry software and its advancement as illustrated through three grand challenge cases for molecular science
The Journal of Chemical Physics **149**, 180901 (2018); 10.1063/1.5052551

Perspective: Dynamics of confined liquids
The Journal of Chemical Physics **149**, 170901 (2018); 10.1063/1.5057759

High and low density patches in simulated liquid water

N. Ansari,[1,a)] R. Dandekar,[2] S. Caravati,[3] G.C. Sosso,[4] and A. Hassanali[1,b)]

[1]*The Abdus Salam International Centre for Theoretical Physics, Strada Costiera 11, 34151 Trieste, Italy*
[2]*The Institute of Mathematical Sciences—HBNI, 4th Cross Street, CIT Campus, Tharamani, Chennai, India*
[3]*Department of Chemistry, University of Zurich, Winterhurerstrasse 190, Zurich CH-8057, Switzerland*
[4]*Department of Chemistry and Centre for Scientific Computing, University of Warwick, Gibbet Hill, Coventry CV4 7AL, United Kingdom*

We present insights into the nature of structural heterogeneities in liquid water by characterizing the empty space within the hydrogen bond network. Using molecular dynamics simulations, we show that density fluctuations create regions of empty space characterized by a diverse morphology – from spherical to fractal-like voids. These voids allow for the identification of low and high density patches of the liquid, encompassing short (0.3-0.5 nm) as well as long (1-2 nm) length-scales. In addition, we show that the formation of these patches is coupled to collective fluctuations involving the topology of hydrogen-bonded rings of water molecules. In particular, water molecules in the high density patches tend to be slightly more tetrahedral – which is consistent with the predictions of the hydrophobic effect. *Published by AIP Publishing.* https://doi.org/10.1063/1.5053559

I. INTRODUCTION

Water is a ubiquitous solvent involved in a wide variety of physical, chemical, and biological processes[1–3] and displays numerous anomalous properties compared to other, simple liquids.[4–10] Understanding the origins of these properties represents a challenge for experiments and theory alike.[11,12] In this regard, the molecular-level details of density fluctuations in water has attracted a lot of attention in the past decades.[13–18] Specifically, fundamental questions regarding the presence and origin of density heterogeneities and the length and time scales over which they occur in water has been a subject of many debates in the literature.[4,8,19–24] A deeper understanding of these aspects is key to further our understanding of phenomena such as the solvation of hydrophobic solutes,[17] protein-folding, and protein-DNA interactions in water.[25]

Small-angle scattering experiments of liquid water have shown the presence of density fluctuations and inhomogeneities occurring on a length scale of 10-15 Å at ambient temperature.[8,12,20] The molecular origins of these medium-range correlations, which lead to characteristic oscillations in the structure factor (see, e.g., discussions around Fig. 3 of Ref. 8), $S(q)$, is still currently debated. These features of the $S(q)$ are often attributed to the co-existence of water molecules forming ordered locally tetrahedral patches (low density liquid—LDL) in equilibrium with water molecules that participate in distorted hydrogen bond patches (high density liquid—HDL).[26] This hypothesis, however, can only be indirectly inferred from experiments and has been the subject of scrutiny by a number of theoretical investigations of bulk liquid water.[21,27–32,86]

Molecular dynamics (MD) simulations examining different order parameters such as the local structure index (LSI),[33] local tetrahedrality (q),[34,35] asphericity of the Voronoi cell,[36] and structure factor,[20,27,37,38] have been used to assess the presence of density inhomogeneities in water at various conditions. The interpretations of these simulations in terms of the existence of the LDL and HDL patches has been heavily contested, with many calculations showing that water is a homogeneous liquid.[21,27–29,39–43] All these studies attempt to characterize LDL and HDL regions using short-range and hence local order parameters.

Herein, Voronoi voids[44] extracted from atomistic simulations are used to show the co-existence of low and high density patches in liquid water on the sub-nanometer and nanometer length scales. By examining the voids and water molecules as a dual network, we identify the presence of spherical and fractal voids. While the spherical voids tend to be localized in space, fractal voids can extend over the nanometer length scale.

The voids allow for the identification of different environments on both the short and long length scale. We show that water in close proximity to the voids forms high density patches similar to the structure of water observed at the air-water interface.[45] Just beyond the high density regions, there exist low density patches involving the clustering of several voids with water molecules interspersed. Our analysis also demonstrates that the formation of both spherical and fractal voids is coupled to the presence of closed rings around the void within a tetrahedral network. In addition, we also examine the behavior of the local LSI and q parameters and find that water molecules in our high density patches tend to be slightly more tetrahedral than those in the low density patches, consistent with the notion that the immediate environment of the voids is hydrophobic.[46] The coupling between the presence of voids and closed rings forming high-density

a)Electronic mail: ansari.narjes@gmail.com
b)Electronic mail: ahassana@ictp.it

patches is not surprising since they resemble thermally excited clathrate-like[19,47] structures in bulk water, within a percolating hydrogen bond network.[39]

These results hold for a diverse array of water models, namely, TIP4P-Ew,[48] SPC/E,[49] TIP4P/2005,[50] and MB-pol.[51–53] Our findings shed light on the interpretation of small-angle x-ray scattering (SAXS)[20,23] and small-angle neutron scattering (SANS)[54] experiments, by providing a comprehensive picture of the water network in terms of collective density fluctuations involving spherical and fractal voids. Besides providing insights into the types of heterogeneities in bulk water, the statistics of void formation in the way that we describe here, is extremely relevant for understanding bubble nucleation at a molecular scale.[55,56]

The paper is organized as follows. After presenting the computational methods used in this work in Sec. II, the characterization of the empty space in water and its consequences on the high and low density patches is discussed in Sec. III. Finally, in Sec. IV, we conclude and give a brief summary and perspectives of our results.

II. COMPUTATIONAL METHODS

Most of our analysis presented here was performed based on classical MD trajectories of bulk water (4096 molecules) obtained via the GROMACS 5.0[57] package. Water molecules have been modeled using the TIP4P-Ew rigid water model.[48] Production runs of 40 ns were performed from which a total of 10^4 configurations were used for analysis, sampled every 4 ps. The equations of motion were integrated using the Verlet algorithm,[58] with a time step of 2 fs. The temperature was kept constant at 270 K by applying a Nose-Hoover thermostat[59,60] with a time constant of 2 ps. This temperature was chosen because the melting temperature T_m of the TIP4P-Ew water model is ~244 K. These simulations were conducted at ambient pressure in the NPT ensemble using the Parrinello-Rahman barostat[61] where the coupling time constant was 1 ps. A cubic box was used with an average side length 49.68 Å. A cutoff of 10 Å was employed for the non-bonded interactions.

We also performed some simulations of water at 1 bar using different water models such as SPC/E,[49] TIP4P/2005,[50] and MB-pol[51–53] in order to examine the sensitivity of our results to the choice of a specific water model. For SPC/E and TIP4P/2005, the average box side lengths were 49.48 Å and 49.67 Å, respectively. The computational parameters for these simulations are the same as those described for TIP4P-Ew. Since the melting temperatures of the SPC/E and TIP4P/2005 models are 215 K and 252.1 K, respectively, we fixed the temperature for the NPT runs to 236 K and 277 K. The MB-pol simulations involved 256 water molecules in a periodic cubic box of side length equal to 19.667 Å using a trajectory of length 1.158 ns.

The voids discussed in this work correspond to the empty regions of space within the water network and have been obtained taking advantage of the framework we have developed and adopted in Ref. 65. Our approach harnesses the concept of the so-called Voronoi S-network, a construction pioneered by Medvedev *et al.*[44,63] and implemented in the Voronoi network poly (VNP) code[64]—which constitute an integral part of our framework (the interested reader is referred to Refs. 62 and 44 for further technical details about our methodology and the Voronoi S-network, respectively).

Voronoi-based approaches are widely used in material science and molecular biology to characterize atomistic models obtained via computer simulations. Applications range from investigation of disordered packings of spheres (liquids and glasses) to complex molecular systems (for example, in membrane proteins). The idea is to assign to a given atom those points in space that are closer to its spherical surface (usually defined according to its van der Waals radius) than to the surfaces of other atoms. The resulting set of points defines a network of cavities which can be tessellated into a collection of tetrahedra. Whether or not two cavities are considered as connected depends on a *bottleneck radius R_B* which quantify the contact area between different cavities. We have assessed the impact of the choice of R_B on the morphology of the voids in previous work devoted to assess the thermodynamics of formation of non-spherical voids in water.[65] Details of how sensitive our results are with respect to the choice of the probe and bottleneck radii will be discussed later in the text. Importantly, the volume of a given void can be straightforwardly obtained as the sum of the volumes of all the tetrahedra involved, while the surface area is simply the sum of the facets of those facets of the tetrahedra which are not in contact with any other facet.

The shape of the voids was characterised by using a set of three different lengths: a, b, and c ($a \geqslant b \geqslant c$). a is the longest distance between any two points forming the surface of the void, b is the longest distance of the vector between any two points forming the surface of the void that is orthogonal to a, and finally c is the longest distance of the vector between any two points forming the surface of the void that is perpendicular to both a and b.

To distinguish between spherical and non-spherical voids, we define two radii as following:

$$R_f = \frac{3V_v}{S_v}, \qquad (1)$$

$$R_v = \left(\frac{3V_v}{4\pi}\right)^{\frac{1}{3}}, \qquad (2)$$

where V_v and S_v correspond to the volume and surface area of the voids, respectively. Their difference $\Delta R = R_f - R_v$ is proportional to the asphericity of the voids and by definition is identical for spherical objects.

The fractal dimensions of our voids d_v and d_s for the volume and surface area, respectively, are defined via the relationship between the volume and surface area [$V_v(r)$ and $S_v(r)$, respectively] and the main tri-axial dimension of the voids where $r = \frac{a}{2}$,

$$V_v(r) \sim r^{d_v}, \qquad (3)$$

$$S_v(r) \sim r^{d_s}. \qquad (4)$$

Note that a perfect sphere would be characterised by $d_v = 3$ and $d_s = 2$.

In order to calculate the running density shown in Fig. 7, $\rho(r_S)$, we define probe volumes around each void so that their shape and dimension is linked to the morphology of the original void. The following strategy was adopted: first, the outward normal vector at the center of each triangular element of the original void was determined. The magnitude of the normal vector (r_S, see the central panel of Fig. 1), which is the distance from the surface of the void is changed from zero to 8 Å for different sizes of probe volumes. The direction of this normal vector during this scaling procedure remains the same. This process leads to the generation of new vertex positions from which new probe volumes can be determined [see panels (a) and (b) of Fig. 1]. Also shown is a visual depiction of the process which clarifies more clearly the construction of the new probe volumes. Note that these probe volumes are closed surfaces that progressively increase as a function of the distance from the original void. In the next step, the vertex points of each new probe volume is used to create a new alpha-shape from which the volume $V(r_S)$ is determined [see panel (c) of Fig. 1]. The concept of the alpha-shape is an approach to formalize the intuitive notion of *shape* for spatial point sets using a generalization of the convex hull and a subgraph of the Delaunay triangulation. The new alpha-shape also provides a convenient way to establish whether a point (in our case, an oxygen atom of a water molecule) lies in or out of the alpha-shape. This needs to be determined in order to calculate the number of waters within the probe volume. In order to construct the alpha-shape, an alpha radius R_α has to be chosen which controls its level of detail. For the probe volume at $r_S = 0$, we have determined R_{α_0} so that the volume of the corresponding alpha-shape is consistent with the volume of the actual void within an accuracy of ± 2 Å^3. The alpha radius for larger probe volumes is chosen as $R_\alpha = R_{\alpha_0} + r_S$. All this analysis was performed using different functions implemented in MATLAB.[66]

In the manuscript, we also examined the ring-statistics around the voids which allows for determining the connectivity of water. Essentially, this analysis looks for the presence of closed rings or loops around the void. Specifically, water molecules either within 2.0 Å of the normal surface of void were accumulated. Thereafter, the longest non-primitive ring was determined using the R.I.N.G.S. code.[62] Non-primitive rings are defined as those that can be decomposed into smaller rings. In order to determine the rings, a geometrical criterion is needed to connect water molecules. For this, a distance cut-off of 3.5 Å between the water molecules was used. In order to assess the extent of hydrogen bonding within the rings, we examined the distribution of O–O bond lengths as well as the H–O–O angle for water molecules forming the rings (see Fig. S4 of the supplementary material). We observe that most of the water molecules are hydrogen bonded based on a geometrical criterion previously defined.[67]

III. RESULTS

A. Voids morphologies

A large number of water configurations (10^3) taken from a 40 ns-long molecular dynamics simulation of TIP4P-Ew water were used to build a Voronoi-Delaunay network[44] from which the voids were constructed. The voids allow for the identification of low and high density patches in the network. We begin by illustrating in Fig. 2 some examples depicting the diverse morphologies of the voids, which encompass fairly spherical as well as highly irregular, even branched topologies. Also shown in Fig. 2 are the length scales associated with representative voids as well as their corresponding volumes. The larger ones involve density fluctuations creating low and high density patches that can extend up to 10 hydrogen bond lengths. Also shown in Fig. 2 is the cumulative distribution of the volumes of the voids where it is clear that the vast majority of the voids in the systems are of small volume and that a small percentage (less than 8% are larger than 100 Å^3).

Panel (a) of Fig. 3 shows the density fluctuations in the simulations which create voids that are anisotropic and can extend beyond 1 nm. This is evident from the long-tail of the bimodal distribution of the dimension a of the voids (see Sec. II for the definition of a).
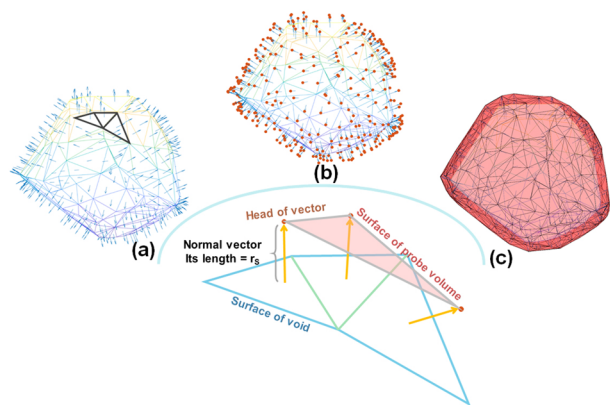

FIG. 1. Three steps to build a probe volume around each void. Details are discussed in the main text. (a) Determination of the outward normal vector at the center of each triangular element of the original void, (b) generation of new vertex positions from these normal vectors to build a new set of positions that encloses the original void, and finally (c) an alpha-shape is constructed based on these new set of positions. Central panel shows a visual depiction of the process which clarifies more clearly the construction of the new probe volumes, from the original triangulation.
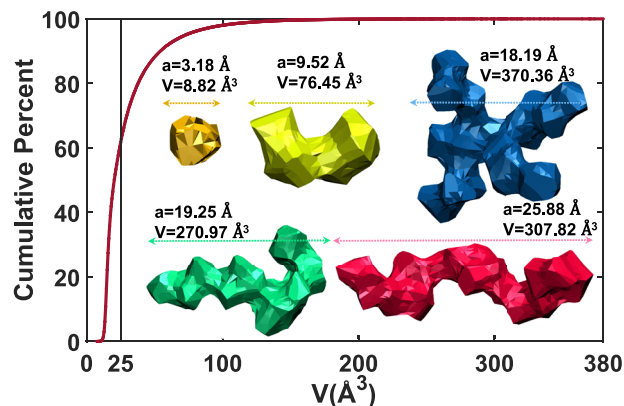

FIG. 2. Cumulative distribution of the volumes of the voids. Inset, representative morphologies of voids in liquid water are shown. The top left corner is a sample of a small spherical void. The remaining voids have a non-spherical morphology. Note the characteristic length scales associated with each void (dashed arrows), which correspond to the length a defined in the main text.
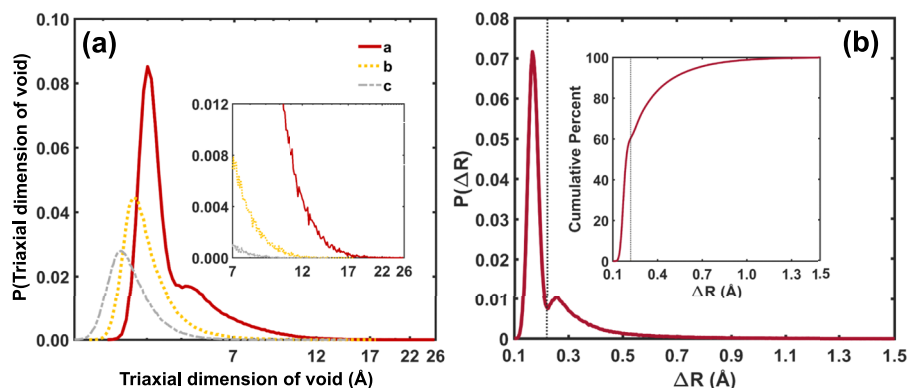
FIG. 3. Evidence of inhomogeneities in void shapes and the existence of spherical and non-spherical voids. (a) Probability distributions of triaxial dimensions *a*, *b*, and *c* averaged over all the voids. The inset shows the dimensions on a log-scale allowing for a more clear signature of the extent of the delocalization of the low density patches in the network. (b) The distribution of ΔR (a parameter that quantifies the spherical or non-spherical character of a void) shown here where the large peak corresponds to more spherical-like voids and the smaller shoulder, non-spherical shapes. The inset shows the cumulative distribution of ΔR. Here, we see that 60% of voids are spherical-like and the 40% are non-spherical voids.

Fig. 2 shows that the vast majority of the voids are spherical with a typical volume of about 25 Å³. Similar to the distribution of the longest dimension *a*, Fig. 3(b) also shows that the distribution of ΔR [Eqs. (1) and (2)] is also bimodal, with a shoulder beyond 0.22 Å showing that density fluctuations indeed lead to a variety of morphologies underpinning two types of voids (spherical and non-spherical) coexisting within the hydrogen bond network.

B. Scaling behavior of voids

The complex morphology of some of these voids strongly suggests the possibility of an underlying fractal structure. Fractals were originally introduced in soft matter physics as a way of characterizing properties of linear and branched polymers,[68,69] and fractal geometry has since been applied to gels, membranes, and various disordered systems.[70,71] The existence of fractal-like cavities in liquids has previously been observed in Monte Carlo simulations by Vishnyakov *et al.*[72] in a confined Lennard-Jones fluid.

Figure 4(a) shows the log-log plot of V_v (see Fig. S1 of the supplementary material for S_v vs. *r*). Note that the volumes of small and large voids scale differently with *r*: for larger voids, a straight-line fit on the log-log plot gives $d_v = 1.69$ [see Eq. (3)], while the surface area dimension is $d_s = 1.52$ [see Eq. (4)]. The two scaling regimes for small and large voids are illustrated in
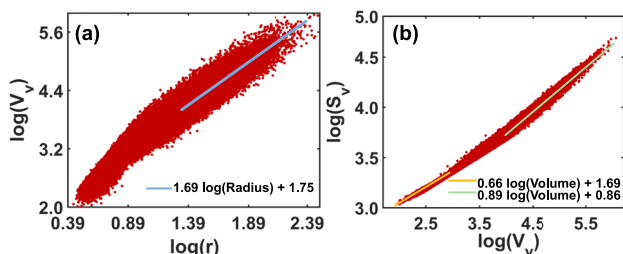
Fig. 4(b), which shows a log-log plot of S_v vs. V_v for all voids. For small voids, $S_v \sim V_v^{0.66}$, which confirms our intuition that in this regime, voids have Euclidean geometry with integer dimension of volume and surface area. For the larger voids, $S_v \sim V_v^{0.89}$, which is in agreement with our measurements for d_s and d_v, as $d_s/d_v = 0.89$.

C. Structural correlations: Water and void network

Before examining how the voids enable the identification of different water environments and high and low density patches, we begin by examining structural correlations between the void and water network. This can be appreciated by constructing pair-correlation functions between water molecules, water and voids, and finally between different voids. For the voids, we use their geometric centre (GC) for the water-void and void-void correlations.

Figure 5 shows the pair correlation functions between the water molecules and voids. Panel (a) of Fig. 5 shows the correlations between water molecules and voids. Perhaps not surprisingly, the water-water and water-void correlations after the first peak are anti-correlated. Essentially, another way to see fluctuations in water density is through the fluctuations of the voids. The behavior in panel (b) of Fig. 5 is less trivial where the void-void correlations are shown. Here we see that the voids tend to cluster and that the density fluctuations involving the voids exhibit weak structuring up to about ~1 nm. The interpretation of SAXS and SANS experiments has relied completely on correlations between water molecules. The evidence here points to more nuanced features associated with the density heterogeneities—this includes, the presence of spherical and fractal voids and their correlations with the surrounding water network. We will see shortly that examining density fluctuations using the dual void-water network representation allows for the identification of heterogeneities on both short and long length scales.

FIG. 4. Behavior of volume and surface area for spherical and fractal voids at short and long length scales, respectively. (a) log-log plot of V_v vs *r*, (b) log-log plot of S_v vs V_v for all voids. The solid lines show best fit slopes for the large volume regime in (a), and both large and small volume regimes in (b).

D. Density fluctuations: High and low density patches

The presence of spherical and fractal voids provides a way to examine density heterogeneities on different length scales in
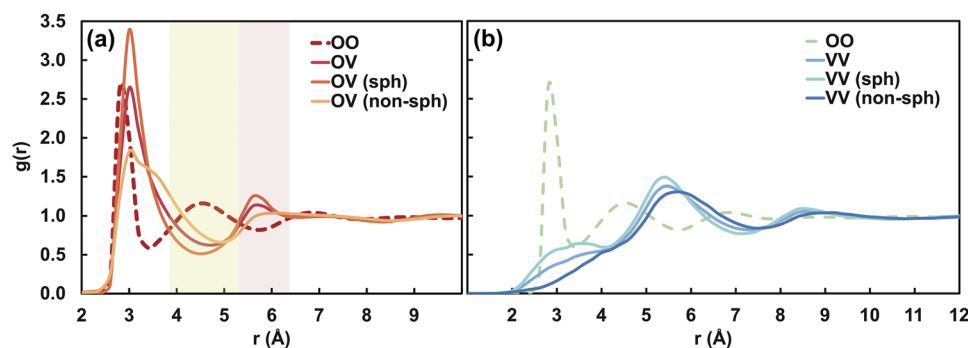
FIG. 5. Pair correlation functions vs distance (r), between (a) void-water (OV) with respect to the geometric centre of a void and (b) void-void between geometric centre of voids (VV). Spherical and non-spherical are referred to as sph and non-sph, respectively. In both panels, the water-water (OO) pair correlation function is shown with a dashed line.

the hydrogen bond network. We begin first by examining how fluctuations in the voids modulate short-range density fluctuations and then subsequently describe how the voids allow for the identification of low and high density patches beyond nearest neighbor.

We begin by first studying the short length-scale density fluctuations. Sitting ourselves on either a water molecule or the geometric centre of a void, we determined the local density (ρ_{local}) computed as number of oxygen atoms inside a probe sphere with radii 4.6 Å. The coupling between ρ_{local} and the number of voids around either the water or void center was then determined. Panels (a) and (b) of Fig. 6 illustrate the coupling between density and void statistics. In both cases, we see clearly that the peak of the density distribution resides around 0.033 molecule/Å^3 representative of bulk density. However, there are fluctuations in the density which are coupled to changes in the shape and the number of voids.

Overall, the local density is negatively correlated with the number of voids both around water and void environments which naturally follows from the fact that the presence of more voids leads to more empty space in the environment. In both panels (a) and (b) of Fig. 6, we also show typical snapshots from the simulations corresponding to different points on the density-void map. What is perhaps interesting in this

analysis is that the molecular origins of bulk-like-density and local fluctuations can originate from different molecular environments. Near a density of 0.033 molecule/Å^3 (labeled 1), the environments leading to this in terms of the size and number of voids is quite different—around the void, water molecules form a cluster that wraps around the cavity, while in the case of a water molecule as the center, one observes a more tetrahedral environment with voids sandwiching the water molecules. Fluctuations to high density creating environments such as that seen in label 3, for example, are even more striking since in the case of the void environment, there is a tightly packed cluster of waters surrounding the central void, whereas in the case of water, the environment is free of any voids. Around both a water molecule and a void, there also appears to be a tail at lower densities and void-number which corresponds to local environments in the proximity of large rarely forming voids.

Next we move on to describing density patches around the voids that describe heterogeneities beyond the first water shell. To this end, we have computed the running density $\rho(r_S)$ around each void which takes into account layers of water molecules that are equidistant from the surface of the void. Figures 7(a) and 7(b) show $\rho(r_S)$ as a function of the distance from the surface of spherical and fractal voids, respectively. More information about how this is computed can be
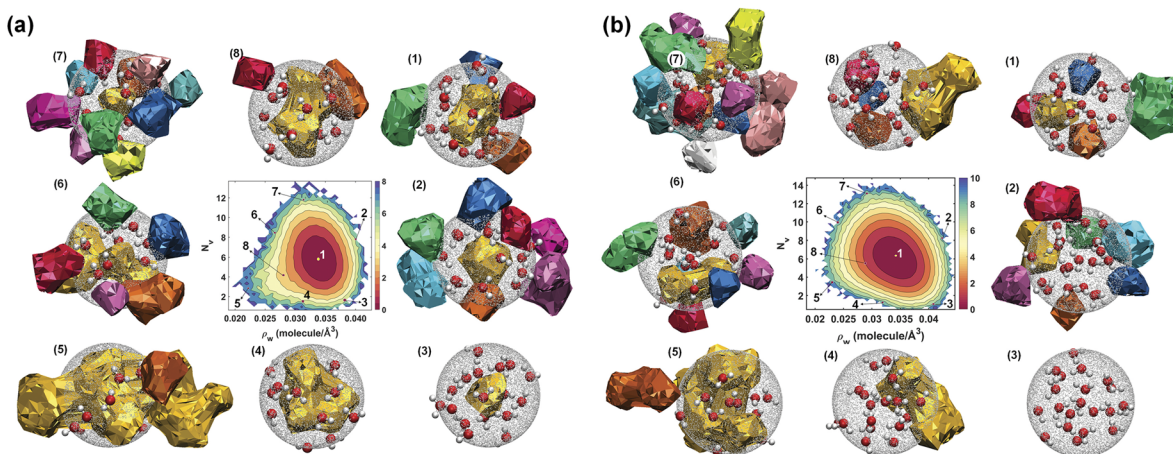

FIG. 6. (a) Central panel shows a two-dimensional distribution of the local density of water around the geometrical center of the void versus the number of voids around this geometrical center (N$_V$). The numbers shown in this distribution correspond to different environments: the pictures around the central panel indicate representative snapshots obtained from the simulation. (b) Similar to (a) except that instead of using the geometric center of the voids, the analysis is repeated sitting on a water molecule. These plots were constructed using a cutoff of 4.6 Å.
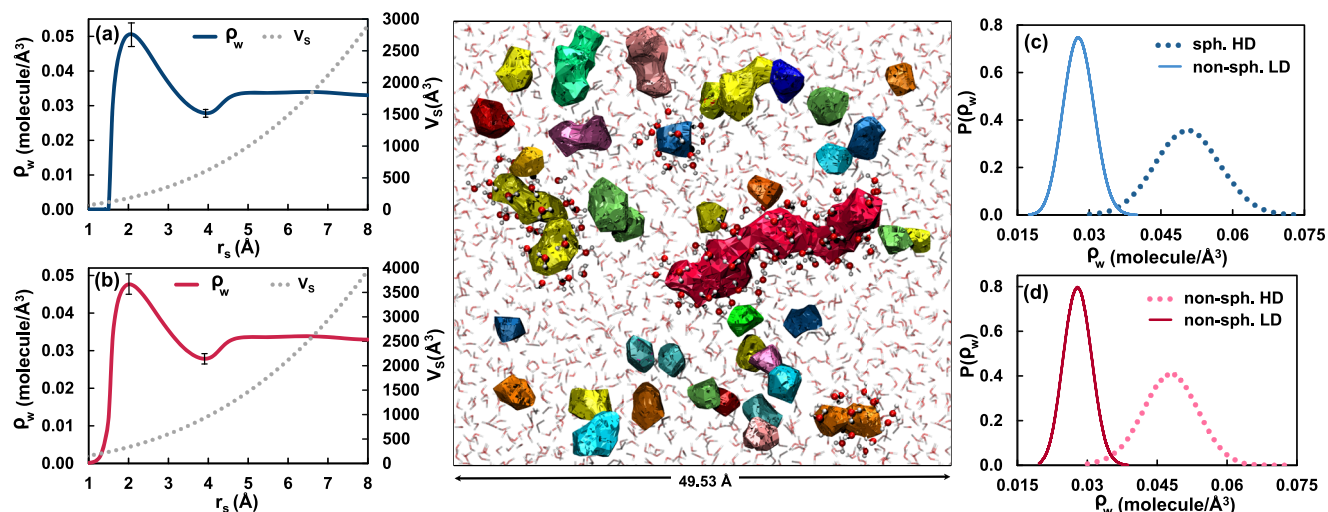
FIG. 7. Existence of high and low density patches around voids. (a) and (b) show the running densities $\rho(r_S)$ and V_S defined in the text, for both spherical and fractal voids. Panels (c) and (d) show the histograms of the distribution of densities near the maximum and minimum for spherical and fractal voids, respectively. The middle panel provides a more qualitative depiction of the voids—see the main text for more details. For three of the voids, we also show using ball and stick representation, water molecules surrounding the void forming a high density patch. Note that this picture reflects an instantaneous frame and that the inhomogeneities would be averaged out over the time scale of several picoseconds. We also note that the large voids shown here are formed very rarely as seen earlier on in Fig. 2 showing the cumulative volume distribution.

found in Sec. II. The running density is defined as $\rho(r_S) = \frac{N_S}{V_S}$, where V_S and N_S correspond to the volume and number of water molecules within the probe volume, respectively. Examining the fluctuations associated with this dual void-water network allows for an identification of low and high density patches. In particular, the analysis summarized in Fig. 7 shows that there exist high density patches in close proximity to the voids. This regime is then followed by low density patches before the bulk like density of 0.033 molecule/Å³ is reached. In Figs. 7(c) and 7(d), the distributions of densities corresponding to the region near the peak at ~2 Å and the minima at 4 Å is shown. For both spherical and fractal voids, the high density region is ~50% larger than the bulk. Later we will rationalize the physical origin of this in terms of the formation of closed rings and how this relates to the local-tetrahedrality.

Besides having a distinct molecular origin, these density patches are different from those previously reported[8,30] since they involve regions of the water network that span much larger volumes. This evidence can be appreciated in Figs. 7(a) and 7(b), where we report the volumes of the voids as a function of r_S. In the case of the fractal voids, the origin of the oscillations in $\rho(r_S)$ involves volumes that are much larger than the volume associated with the first hydration sphere of water (~215 Å³) which is typically used to describe low and high density regions, for example, using the LSI or tetrahedrality index. For reference, we also examined the voids distribution and density patches from a configuration of hexagonal ice (see supplementary material for details). Interestingly, we see that hexagonal ice is dominated by spherical-like voids only. Examining the running density around the voids also reveals a similar behavior as was observed in the voids in the liquid, except that there is more structuring as expected in the crystalline phase. The co-existence of the low and high density patches is qualitatively described in the middle of

Fig. 7 which shows a slice in the XY plane of our water box. Some of the colored voids are highlighted to show different types of voids along with the high density patches of water molecules that form around them. This qualitative description is reminiscent, but conceptually distinct, from some of the ideas proposed by Nilsson and Petterson in a recent review.[8] It should be stressed again that the middle panel is an instantaneous frame and that on a time scale of several picoseconds these inhomogeneities would be averaged out at room temperature.

E. Density patches and water network parameters

1. Ring analysis

The creation of low and high density patches around the voids suggests a collective effect involving the fluctuations of the hydrogen bond network. To examine this more closely, we searched for closed rings[30,32,73–77] of hydrogen-bonded water molecules, which represent continuous connections of water molecules around the voids. Figure 8 shows the probability distributions, P(N), of the N-membered rings that form within the first molecular layer of water around high density patches for spherical and fractal voids. Interestingly, we see that for both types of voids, there are water molecules forming rings: in the case of fractal voids, however, the distribution is characterized by a broader distribution involving the formation of extended networks of hydrogen bond connections between water molecules forming water wires analogous to the surface of water that was previously studied in our group.[87] In the current work, however, the water wires spread out in three dimensions. Thus the presence of a high density patch is correlated with the formation of closed rings. The low density patches adjacent to these rings consist of a clustering of several voids—with water molecules in between them but do not form rings.
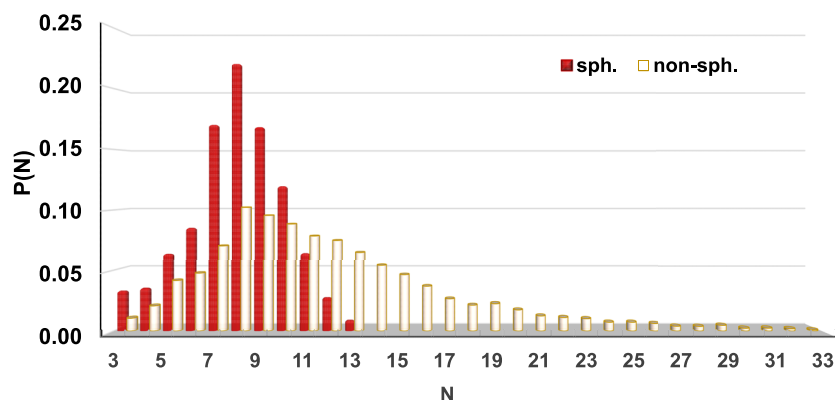
FIG. 8. Coupling of water network and the presence of spherical and fractal voids. Probability distribution of N-membered rings that are found within the high density patch around both spherical and fractal voids. Increasing the threshold of the shell naturally results in the formation of larger sized rings. However, the fractal voids are always characterized by larger sized rings—see Fig. S3 of the supplementary material for details.

2. Tetrahedrality and local structure index

One of the cornerstones of the hydrophobic effect in water is that the presence of a hydrophobic molecule results in some form of structuring of the water molecules close to its vicinity.[46,78–81] This is due to the fact that water tries to form stronger inter-hydrogen bonds. In order to assess how the local structure of water molecules behaves around the voids, we computed the tetrahedrality (q) for water molecules that lie in the high density patch in the regime where the local density is equal or higher than 0.0429 molecule/Å^3. This corresponds to the density that is 30% larger than the bulk density. These waters essentially correspond to water molecules that form the closed rings around the voids. In addition, we also examined the LSI parameter for these waters.

Figures 9(a) and 9(b) compares the distributions of the tetrahedrality and LSI for waters that reside in the HD patches as described earlier, to all the other water molecules. Interestingly, we observe that the tetrahedrality for water molecules in the high density patch of the voids (waters@HDP) is slightly larger than all the other waters (waters-HDP). Although it is a rather subtle effect, this is consistent with the idea that the voids represent hydrophobic objects and hence the water molecules surrounding the voids in the closed rings tend to have a slight bias to being more tetrahedral.[46] The existence of more tetrahedral-like waters within the high density patch around the voids may seem rather counterintuitive. This is because the literature typically refers to low density liquid (LDL) as being characterized by more open, ice-like, and hence tetrahedral structure. On the other hand, high density liquid (HDL)
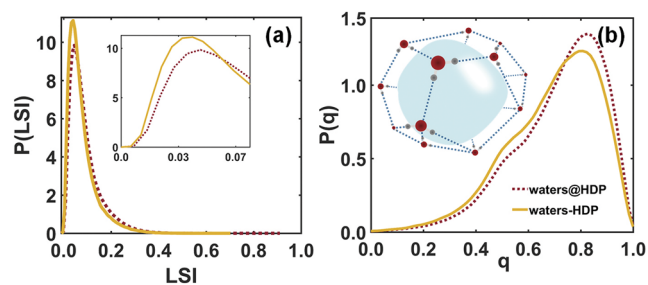
involves a more disordered first solvation shell which is less tetrahedral. The definition and origin of our density patches is fundamentally different: it is a non-local definition that extends over several solvation shells and involves a network of closed rings that form around the void (see Fig. S5 of the supplementary material). What is rather interesting is that they resemble thermally excited clathrate-like[47] structures within a percolating hydrogen bond network [see the cartoon scheme in the inset of Fig. 9(b)]. The water molecules within the high density patch are akin to those near non-polar hydrophobic solutes and hence it is not surprising that they are slightly more tetrahedral. An analysis of the LSI parameter also confirms this behavior—water molecules in the high density patch with higher tetrahedrality tend to have a slightly larger LSI value implying a more ordered first shell environment.[30] It is also akin to previous simulations by Molinero and co-worker[82]

FIG. 9. Distribution of (a) LSI and (b) q for waters in the patches (waters@HDP) with density equal or greater than 0.0429 molecule/Å^3 (which corresponds to a density that is 30% larger than bulk) and all the other water molecules (waters-HDP). Cartoon inset of panel (b) defined in the main text.
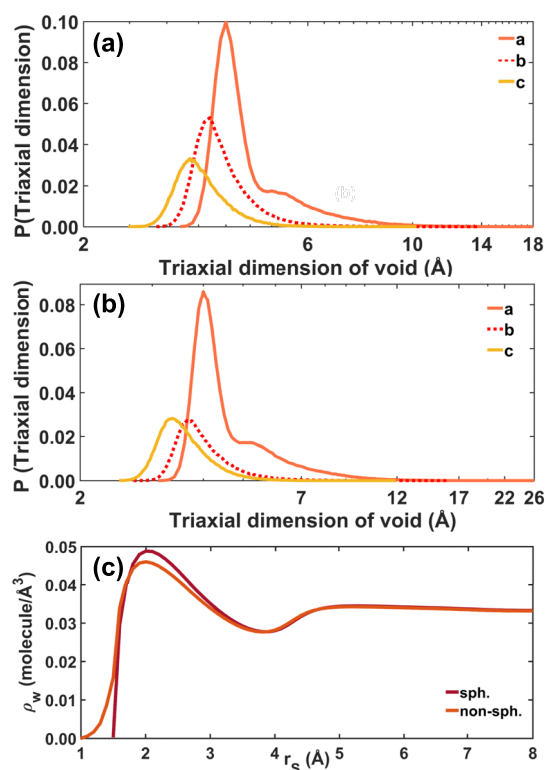
FIG. 10. Distribution of triaxial dimension of voids for (a) MB-pol and (b) SPC/E water models. (c) Running densities $\rho(r_S)$ defined in the text, for both spherical and fractal voids for MB-pol water model.
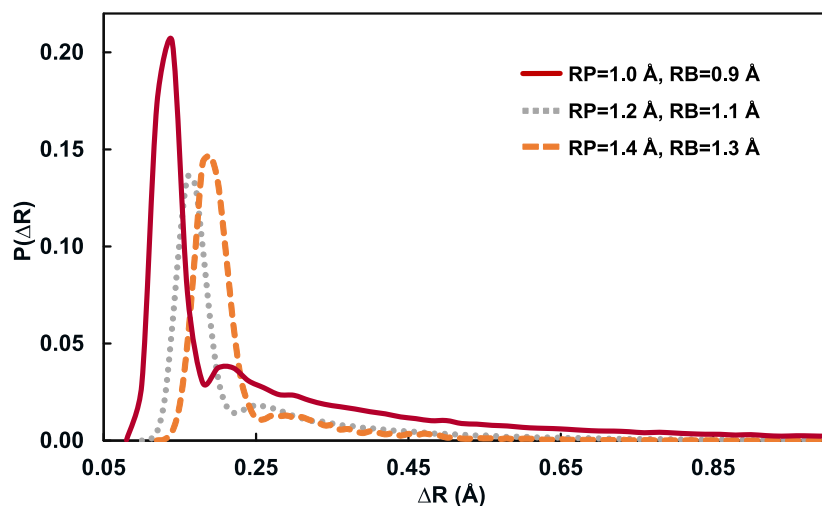
FIG. 11. The distribution of ΔR for MB-pol water model with the probe radii (RP) 1.1 ± 0.2 Å and bottleneck radii (RB) 1.1 ± 0.2 Å, respectively.

who have shown a growing correlation length involving long-range structural fluctuations of patches of four-coordinated molecules as one goes into the supercooled regime.

F. Void statistics: Sensitivity to parameters and water models

All the analysis of the voids presented here was done using the TIP4P-Ew water model. We wanted to assess the sensitivity of our results to the choice of the water model and hence also performed some benchmarks using a series of different water models, namely, SPC/E, TIP4P/2005, and MB-pol. Figure 10 shows the resulting triaxial dimension distributions for two of the water models, namely, MB-pol and SPC/E. For neat water, MB-pol provides the most accurate thermodynamic and dynamical description of water across the phase diagram. We see clearly that the distributions of the tri-axial axes are very similar for both MB-pol and SPC/E and compare well to what we obtain with TIP4P-Ew. In the case of MB-pol, the smaller box size implies that we do not sample as large voids as we do with SPC/E and TIP4P/Ew.

Earlier in Fig. 7, we showed that the voids allow for the identification of high and low density patches which was illustrated for TIP4P/Ew. Panel (c) of Fig. 10 shows the density around spherical and fractal voids obtained from the MB-pol simulations. Again, it is clear that the presence of the high and low density patches around the voids is reproduced by all water models.

As alluded to in Sec. II, the construction of the voids relies on two key parameters, namely, the probe and bottleneck radii. The probe and bottleneck radii used to construct the voids reported in the paper were 1.2 Å and 1.1 Å, respectively. The probe radii is the smaller of the van der Waals radii of oxygen and hydrogen, while the bottleneck radius is chosen in such a manner that the bottlenecks have to be larger than 2×1.1 Å, an extent that is large enough to accommodate a hydrogen-hydrogen distance of a water molecule.

In order to check the robustness of our results, in particular, the bi-modal character observed in Fig. 3, we reconstructed $P(\Delta R)$ altering the bottleneck and probe radii. This analysis was performed for the MB-pol trajectory. Figure 11 shows how our ΔR parameter varies when these two parameters are changed—while there are obvious quantitative changes in the ratio of fractal to spherical voids, the qualitative picture still remains robust.

IV. CONCLUSIONS

In this work, we have used Voronoi voids as an order parameter to examine density heterogeneities in simulated liquid water. What makes our analysis unique is that the voids allow for the identification of low and high density patches on a much larger length scale than those reported previously. In many ways, the coupling of the voids and the surrounding water are another way to describe the transient formation of clathrate-like structures in the liquid. It is important to stress that the density patches depicted in the middle panel of Fig. 7 do not imply the co-existence of two distinct phases at the thermodynamic conditions we have currently simulated. As pointed out in previous studies, water is still a homogeneous liquid on average.

An immediate question that our theoretical predictions pose is how to experimentally probe the spherical and fractal voids and the correlations that exist between them as seen in Fig. 5. While this is a challenging problem, our findings should serve as motivation for novel development of application of experimental techniques to probe the voids in the network. It would also be interesting in the future to understand how the collective density fluctuations as we have shown here are related to the existing work on optical[83] and acoustic[84] modes in water. We are also acutely aware that results here come from an analysis of simulated water and we cannot rule out the possibility that there are still limitations in the current models. However, it is comforting to see that the void analysis we perform is reproduced in all water models simulated.

While we have focused on density fluctuations in water at ambient conditions, one of the obvious extensions would be to examine density inhomogeneities in the supercooled region of water and how it relates to the density patches that we observe. Such insights could in turn provide the key to understand the molecular origins of the glass transition—perhaps in the context of free-volume theory.[85]

SUPPLEMENTARY MATERIAL

See supplementary material for surface area scaling (TIP4P/EW), distribution of number of voids (high, low, and bulk density regimes), and ring distributions.

ACKNOWLEDGMENTS

[1]D. Eisenberg and W. Kauzmann, *The Structure and Properties of Water*, Oxford Classic Texts in the Physical Sciences (OUP Oxford, 2005).

[2]P. Ball, Chem. Rev. **108**, 74 (2008).

[3]M.-C. Bellissent-Funel *et al.*, Chem. Rev. **116**, 7673 (2016).

[4]P. Wernet *et al.*, Science **304**, 995 (2004).

[5]C. A. Angell, Science **319**, 582 (2008).

[6]S. Woutersen, B. Ensing, M. Hilbers, Z. Zhao, and C. A. Angell, Science **359**, 1127 (2018).

[7]C. A. Angell, *Water: A Comprehensive Treatise*, edited by F. Franks (Plenum, New York, 1982), Vol. 7.

[8]A. Nilsson and L. G. Pettersson, Nat. Commun. **6**, 8998 (2015).

[9]O. Mishima and H. E. Stanley, Nature **396**, 329 (1998).

[10]P. G. Debenedetti, J. Phys.: Condens. Matter **15**, R1669 (2003).

[11]P. Gallo *et al.*, Chem. Rev. **116**, 7463 (2016).

[12]L. G. M. Pettersson, R. H. Henchman, and A. Nilsson, Chem. Rev. **116**, 7459 (2016).

[13]T. Yagasaki and S. Saito, Annu. Rev. Phys. Chem. **64**, 55 (2013).

[14]I. Ohmine and S. Saito, Acc. Chem. Res. **32**, 741 (1999).

[15]A. J. Patel, P. Varilly, D. Chandler, and S. Garde, J. Stat. Phys. **145**, 265 (2011).

[16]J. Mittal and G. Hummer, Proc. Natl. Acad. Sci. U. S. A. **105**, 20130 (2008).

[17]D. Chandler, Nature **437**, 640 (2005).

[18]K. Lum, D. Chandler, and J. D. Weeks, J. Phys. Chem. B **103**, 4570 (1999).

[19]T. Head-Gordon and M. E. Johnson, Proc. Natl. Acad. Sci. U. S. A. **103**, 7973 (2006).

[20]C. Huang, K. T. Wikfeldt, T. Tokushima, D. Nordlund, Y. Harada, U. Bergmann, M. Niebuhr, T. M. Weiss, Y. Horikawa, M. Leetmaa *et al.*, Proc. Natl. Acad. Sci. U. S. A. **106**, 15214 (2009).

[21]G. N. Clark, C. D. Cappa, J. D. Smith, R. J. Saykally, and T. Head-Gordon, Mol. Phys. **108**, 1415 (2010).

[22]L. G. Pettersson and A. Nilsson, J. Non-Cryst. Solids **407**, 399 (2015).

[23]F. Perakis, K. Amann-Winkel, F. Lehmkühler, M. Sprung, D. Mariedahl, J. A. Sellberg, H. Pathak, A. Späh, F. Cavalca, D. Schlesinger *et al.*, Proc. Natl. Acad. Sci. U. S. A. **114**, 8193 (2017).

[24]H. V. Colot, G. Park, G. E. Turner, C. Ringelberg, C. M. Crew, L. Litvinkova, R. L. Weiss, K. A. Borkovich, and J. C. Dunlap, Proc. Natl. Acad. Sci. U. S. A. **103**, 10352 (2006).

[25]Y. Levy and J. N. Onuchic, Annu. Rev. Biophys. Biomol. Struct. **35**, 389 (2006).

[26]R. Dandekar and A. A. Hassanali, Phys. Rev. E **97**, 062113 (2018).

[27]G. N. Clark, G. L. Hura, J. Teixeira, A. K. Soper, and T. Head-Gordon, Proc. Natl. Acad. Sci. U. S. A. **107**, 14003 (2010).

[28]A. K. Soper, Pure Appl. Chem. **82**, 1855 (2010).

[29]E. Duboue-Dijon and D. Laage, J. Phys. Chem. B **119**, 8406 (2015).

[30]B. Santra, R. A. DiStasio, Jr., F. Martelli, and R. Car, Mol. Phys. **113**, 2829 (2015).

[31]P. Hamm, J. Chem. Phys. **145**, 134501 (2016).

[32]J. Liu, X. He, and J. Z. Zhang, Phys. Chem. Chem. Phys. **19**, 11931 (2017).

[33]E. Shiratani and M. Sasai, J. Chem. Phys. **104**, 7671 (1996).

[34]P.-L. Chau and A. Hardwick, Mol. Phys. **93**, 511 (1998).

[35]J. R. Errington and P. G. Debenedetti, Nature **409**, 318 (2001).

[36]G. Ruocco, M. Sampoli, and R. Vallauri, J. Chem. Phys. **96**, 6167 (1992).

[37]S. Overduin and G. Patey, J. Phys. Chem. B **116**, 12014 (2012).

[38]K. T. Wikfeldt, C. Huang, A. Nilsson, and L. G. Pettersson, J. Chem. Phys. **134**, 214506 (2011).

[39]F. H. Stillinger, Science **209**, 451 (1980).

[40]N. J. English and S. T. John, Phys. Rev. Lett. **106**, 037801 (2011).

[41]M. Matsumoto, Phys. Rev. Lett. **103**, 017801 (2009).

[42]S. Overduin and G. Patey, J. Chem. Phys. **138**, 184502 (2013).

[43]P. Gasparotto, A. A. Hassanali, and M. Ceriotti, J. Chem. Theory Comput. **12**, 1953 (2016).

[44]M. G. Alinchenko, A. V. Anikeenko, N. N. Medvedev, V. P. Voloshin, M. Mezei, and P. Jedlovszky, J. Phys. Chem. B **108**, 19056 (2004).

[45]A. P. Willard and D. Chandler, J. Phys. Chem. B **114**, 1954 (2010).

[46]X. Wu, W. Lu, L. M. Streacker, H. S. Ashbaugh, and D. Ben-Amotz, J. Phys. Chem. Lett. **9**, 1012 (2018).

[47]T. Head-Gordon, Proc. Natl. Acad. Sci. U. S. A. **92**, 8308 (1995).

[48]H. W. Horn, W. C. Swope, J. W. Pitera, J. D. Madura, T. J. Dick, G. L. Hura, and T. Head-Gordon, J. Chem. Phys. **120**, 9665 (2004).

[49]H. Berendsen, J. Grigera, and T. Straatsma, J. Phys. Chem. **91**, 6269 (1987).

[50]J. L. Abascal and C. Vega, J. Chem. Phys. **123**, 234505 (2005).

[51]V. Babin, G. R. Medders, and F. Paesani, J. Phys. Chem. Lett. **3**, 3765 (2012).

[52]V. Babin, C. Leforestier, and F. Paesani, J. Chem. Theory Comput. **9**, 5395 (2013).

[53]G. R. Medders, V. Babin, and F. Paesani, J. Chem. Theory Comput. **10**, 2906 (2014).

[54]D. Liu, Y. Zhang, C.-C. Chen, C.-Y. Mou, P. H. Poole, and S.-H. Chen, Proc. Natl. Acad. Sci. U. S. A. **104**, 9570 (2007).

[55]V. K. Shen and P. G. Debenedetti, J. Chem. Phys. **118**, 768 (2003).

[56]G. Menzl and C. Dellago, J. Chem. Phys. **145**, 211918 (2016).

[57]M. J. Abraham, T. Murtola, R. Schulz, S. Páll, J. C. Smith, B. Hess, and E. Lindahl, SoftwareX **1**, 19 (2015).

[58]R. Hockney, S. Goel, and J. Eastwood, J. Comput. Phys. **14**, 148 (1974).

[59]W. G. Hoover, Phys. Rev. A **31**, 1695 (1985).

[60]S. Nosé and M. Klein, Mol. Phys. **50**, 1055 (1983).

[61]M. Parrinello and A. Rahman, J. Appl. Phys. **52**, 7182 (1981).

[62]S. Le Roux and P. Jund, Comput. Mater. Sci. **49**, 70 (2010).

[63]N. N. Medvedev, V. Voloshin, V. Luchnikov, and M. L. Gavrilova, J. Comput. Chem. **27**, 1676 (2006).

[64]See http://www.kinetics.nsc.ru/mds/?Software:VNP for The VNP code; accessed 5 July 2016.

[65]G. C. Sosso, S. Caravati, G. Rotskoff, S. Vaikuntanathan, and A. Hassanali, J. Phys. Chem. A **121**, 370 (2016).

[66]MATLAB and statistics toolbox Release 2017a, The Mathworks, Inc., Natick, Massachusetts, USA, 2017.

[67]A. Luzar and D. Chandler, Nature **379**, 55 (1996).

[68]S. Havlin and D. Ben-Avraham, J. Phys. A: Math. Gen. **15**, L311 (1982).

[69]H. E. Stanley, J. Stat. Phys. **36**, 843 (1984).

[70]L. Pietronero and E. Tosatti, *Fractals in Physics* (Elsevier, 2012).

[71]A. Bunde and S. Havlin, *Fractals in Science* (Springer, 2013).

[72]A. Vishnyakov, P. G. Debenedetti, and A. V. Neimark, Phys. Rev. E **62**, 538 (2000).

[73]A. Rahman and F. Stillinger, J. Am. Chem. Soc. **95**, 7943 (1973).

[74]A. Hassanali, F. Giberti, J. Cuny, T. D. Kühne, and M. Parrinello, Proc. Natl. Acad. Sci. U. S. A. **110**, 13723 (2013).

[75]Y. Ding, A. A. Hassanali, and M. Parrinello, Proc. Natl. Acad. Sci. U. S. A. **111**, 3310–3315 (2014).

[76]A. A. Hassanali, F. Giberti, G. C. Sosso, and M. Parrinello, Chem. Phys. Lett. **599**, 133 (2014).

[77]I. Bakó, Á. Bencsura, K. Hermannson, S. Bálint, T. Grósz, V. Chihaia, and J. Oláh, Phys. Chem. Chem. Phys. **15**, 15163 (2013).

[78]J. Grdadolnik, F. Merzel, and F. Avbelj, Proc. Natl. Acad. Sci. U. S. A. **114**, 322 (2017).

[79]H. S. Frank and M. W. Evans, J. Chem. Phys. **13**, 507 (1945).

[80]W. Kauzmann, *Advances in Protein Chemistry* (Elsevier, 1959), Vol. 14, pp. 1–63.

[81]R. Haselmeier, M. Holz, W. Marbach, and H. Weingaertner, J. Phys. Chem. **99**, 2243 (1995).

[82]E. B. Moore and V. Molinero, J. Chem. Phys. **130**, 244505 (2009).

[83]D. C. Elton and M. Fernández-Serra, Nat. Commun. **7**, 10193 EP (2016).

[84]S. Santucci, D. Fioretto, L. Comez, A. Gessini, and C. Masciovecchio, Phys. Rev. Lett. **97**, 225701 (2006).

[85]R. Zallen, *The Physics of Amorphous Solids* (John Wiley & Sons, 2008).

[86]J. R. Errington, P. G. Debenedetti, and S. Torquato, Phys. Rev. Lett. **89**, 215503 (2002).

[87]F. Giberti and A. Hassanali, J. Chem. Phys. **146**, 244703 (2017).